\$ SUPER

Contents lists available at ScienceDirect

Environmental Research

journal homepage: www.elsevier.com/locate/envres





Plastic litter fate and contaminant transport within the urban environment, photodegradation, fragmentation, and heavy metal uptake from storm runoff

Md Hadiuzzaman ^a, Maryam Salehi ^{a,*}, Tomoko Fujiwara ^b

- ^a Department of Civil Engineering, The University of Memphis, Memphis, TN, USA
- b Department of Chemistry, The University of Memphis, Memphis, TN, USA

ARTICLE INFO

Keywords:
Microplastics
Litter
Environmental weathering
Fragmentation
Heavy metals
Stormwater

ABSTRACT

A significant portion of urban litter is plastic which contaminates the environment and threatens ecological safety. The conversion of plastic litter into small fragments called microplastics (MPs) intensifies their critical risks by facilitating their transport and altering their physicochemical features. This study focuses on low density polyethylene (LDPE) and polyethylene terephthalate (PET) as the main components of urban litter. The photodegradation of LDPE and PET MPs due to the accelerated weathering experiments is investigated through surface chemistry and morphology analysis. The influence of MPs' photodegradation on their fragmentation behavior is evaluated through the innovative accelerated mechanical weathering experiments that simulated the abrasion of MPs with the road deposits. Furthermore, the role of MPs as the vehicles to transport the heavy metals from the urban environment to the water resources is evaluated by studying the kinetics of lead (Pb) uptake by new and weathered MPs in synthetic stormwater. The surface morphology investigation revealed the formation of crazes and the crack networks onto the MPs due to the weathering experiments. The surface chemistry analysis revealed the generation of several oxidized carbon surface functional groups onto the photodegraded MPs and their increased susceptibility to fragmentation due to the abrasion with the road deposits. The photodegradation increased the Pb accumulation onto the LDPE and PET MPs from 467 μ g/m² and 21 μ g/m² to 2290 $\mu g/m^2$ and 725 $\mu g/m^2$, after five days of metal exposure. The fundamental knowledge developed in this research provides a better conceptual understanding of the mechanisms controlling MPs persistence and contaminant transport within the urban environment, which is crucial to estimate their negative impacts on the ecosystem.

1. Introduction

Littering within the urban area is a global problem with aesthetic, economical, and environmental impacts (Schultz et al., 2013). It was estimated to have around 50 billion of litter pieces around the roadways and water ways in the U.S., which counts as 152 pieces of litter per each U.S. resident (Scott et al., 2020). A significant portion of this litter is plastic, which unlike the food scrape and paper wraps dose not decompose readily and rapidly. This is alarming as plastic production has grown rapidly from 1.5 million tons annually in 1945 to 359 million tons in 2019 (Lundquist et al., 2000). Moreover, the COVID-19 pandemic and the urgent need for disposable personal hygiene products and disposable supplies has intensified the plastic pollution

problem (Tesfaldet et al., 2022). Due to COVID-19 pandemic, the personal protective equipment (PPE) demand increased worldwide (Shams et al., 2021; Abdolazimi et al., 2021). For instance, in the U.S., the estimated monthly demand for face masks has raised to 129 billion (Patrício Silva et al., 2021). Furthermore, the U.S., medical plastic waste increased by six-folds to 8.85 million tons at the end of 2020 (Shams et al., 2021).

Plastic litter exposure to the external mechanical forces within the urban environment such as vehicles passing the litters, entanglement to the trees/plants or urban structures, and stresses caused by the wind action may result in their conversion to the small fragments called microplastics (MPs). The MPs smaller size compared to the original litter could facilitate their transport via wind or storm runoff. Thus, rather

^{*} Corresponding author. 108 Engineering Science Building, University of Memphis, Memphis, TN, 38152., *E-mail addresses*: mssfndrn@memphis.edu, msalehiesf@gmail.com (M. Salehi).

than potential risk toward the terrestrial ecosystem, they can impact the aquatic systems or expose the human through inhalation and ingestion (Wright and Kelly, 2017). The literature suggests that stormwater from urban areas and highways is among the major routes conveying MPs from land sources to surface waters (Piñon-Colin et al., 2020). Stormwater retention ponds have been reported as hotspots for MPs accumulation and their critical role in transporting MPs to the aquatic environment (Liu et al., 2019). The presence of MPs in urban storm runoff threatens the aquatic environment and endangers human health (Dehghani et al., 2017). Rather than physical threats caused by the MPs, they can release toxic chemicals and accumulate other contaminants (Devriese et al., 2017). Having the water shortage crises growing worldwide, it's critical to protect the safety of our freshwater resources (Salehi, 2022).

The MPs exposure to solar radiation as they are left within the urban environment could alter their physiochemical characteristics and their subsequent fragmentation behavior. A growing number of studies have been conducted to quantify the MPs fragmentation under different environmental conditions (Chubarenko et al., 2020; Lambert and Wagner, 2016; Enfrin et al., 2020). Song et al. (2017) studied combined effect of UV and mechanical degradation of low-density polyethylene (LDPE), polypropylene (PP), and expanded polystyrene (EPS) within the simulated beach environment (Song et al., 2017). Julienne et al., 2019 studied fragmentation of LDPE film due to photodegradation in air and water (Julienne et al., 2019). Chubarenko et al. (2020) examined fragmentation behavior of sinking polystyrene (PS), flexible LDPE, foamed PS, and buoyant PP simulating sea swash region with natural beach sediments (Chubarenko et al., 2020). Mechanical degradation is critical as it influences the fragmentations of MPs to smaller fractions and impacts their sinking and buoyancy behavior (Kowalski et al., 2016). Several studies have reported accumulation of MPs within the road deposits (Vogelsang et al., 2018; Su et al., 2020), however, the extent of MPs fragmentation due to the abrasion by the silt and sand particles present within the road deposit is still unknown. The MPs present within the road deposits around the roadways and water ways could be transported via stormwater runoff to the water resources (Ballent et al., 2016). MPs environmental degradation may impact the propensity of MPs to accumulate contaminants and transport them over long distances (Holmes et al., 2012). Our recent study revealed an increased Pb accumulation onto the low density polyethylene (LDPE) pellets that were aged by ozonation compared to the new LDPE pellets (Huang et al., 2020; Salehi et al., 2018). The literature has reported elevated concentration of heavy metals such as Ni, Cu, Pb, Zn on parking lots and paved roads due to the vehicle emissions (Geronimo et al., 2014). On the other hand, lots of plastic fragments may also be found within this area due to the common plastic littering. The stormwater could wash off both these contaminant and transport them to the surrounding water resources (Salehi et al., 2020), despite a significant literature on marine environment, a very limited understanding is available on the interaction of new and weathered MPs with heavy metals in stormwater. In this study lead (Pb) was selected as a model heavy metal due to its significant health impacts and toxicity toward the aquatic organisms (DeSimone et al., 2020).

This study aims to better understand the fate and contaminant transport behavior of plastic litter within the urban environment. The specific objectives are to (1) Investigate the degree of surface chemistry, and morphology changes of LDPE and PET MPs due to the photodegradation, (2) Examine the influence of MPs' photodegradation on their fragmentation behavior due to their simulated abrasion with the road deposits, and (3) Investigate the critical role of MPs weathering on their Pb uptake in stormwater. LDPE and PET were selected as they are two of the most common manufactured non-biodegradable thermoplastics in the world, widely used as disposable plastic bags and beverage bottles (Martín et al., 2017; Aghilinasrollahabadi et al., 2020). This research particularly targets the plastic pollutants within the urban environment and customizes the fragmentation investigations to

simulate the conditions where microplastics are abraded with the sediments present within the road deposits. Linking the MPs' photodegradation to their heavy metals transport within the storm runoff is another innovative aspect of this research that underscores the potential environmental risks associated with plastic pollution within the urban environment.

2. Experimental

2.1. Materials

The LDPE and PET films (thickness 0.01 cm) were purchased from McMaster-Carr, USA. The Lead (Pb) ICP-MS standard (1000 mg/L in 3% nitric acid) was purchased from RICCA Chemical Company (Arlington, TX, USA). Sodium Chloride (NaCl), Zinc Chloride (ZnCl₂), and Nile Red were purchased from Fisher Scientific (Waltham, MA, USA). Whatman No. 1 filter paper of pore size 1.2 μ m and 11 μ m were purchased online from Cole-Parmer, USA. Ultrapure Milli-QTM (18 M Ω *cm) treated water was used for conducting all the experiments. The particle size for the sand used for mechanical fragmentation varied between 425 μ m and 1000 μ m. The sand was pretreated before the experiments, as described elsewhere (Aghilinasrollahabadi et al., 2020).

2.2. Accelerated degradation experiments

The QUV accelerated weathering tester (Model: QUV, Serial No.: 84-2132-27, Volts: 120, Hz: 60, Watts: 1200, The Q-Panel Company, Ohio, USA) was utilized for the accelerated photodegradation experiments. Ultraviolet B (UVB) radiation extends from around 280 nm–315 nm wavelength within the UV spectrum. The UVB bulbs with wavelength 313 nm were used to accelerate the degradation of the plastic films as this radiation wavelength simulates the UVB radiation of the sunlight. More information is provided in SI-1. For accelerated mechanical degradation experiments, 10 g of sand was added to 250 mL of an amber glass bottle containing a single 0.5 cm \times 0.5 cm square-sized LDPE or PET MPs sample. An Amber glass bottle was used to prevent further photo exposure to the MPs. Three replicates were used for each condition. The bottles were shaken by a Lab-Line Orbital Shaker (Lab-line Instruments Inc.) for 28 days at 200 rpm at room temperature.

2.3. Quantification of plastic fragments

The plastic fragments generated by accelerated mechanical degradation of LDPE and PET samples were separated from the sand by floating in a NaCl solution (density of $1.2~\rm g/cm^3$) (Song et al., 2017) and ZnCl $_2$ solution (density of 1.5– $1.7~\rm g/cm^3$), respectively (Imhof et al., 2012). Fragmented MPs were filtered using filter paper (pore size of $1.2~\rm \mu m$) and stained with Nile Red solution (5 mg/L Nile Red in hexane) on the filter paper. The fluorescence microscope was a Nikon A1R laser confocal scanning fluorescence microscope with 488 nm excitation and 568 nm solid-state lasers for emission and photomultiplier tubes (PMT) to collect emitted light. The images were analyzed with the ImageJ (version, 1.53a) software to count the number of fragmented MPs. The MPs quantification method utilized in this research was able to quantify the MPs with the size range of $10~\rm \mu m$ – $120~\rm \mu m$. More information regarding the quantification and control samples is provided in SI-2.

2.4. Surface chemistry characterizations

The surface chemistry characterization was conducted for photodegraded MPs. The ATR-FTIR transmission spectra were recorded using a PerkinElmer Universal Attenuated Total Reflectance Fourier transform infrared spectroscopy (ATR-FTIR) spectrophotometer from 4000 to 650 cm⁻¹ with a 4 cm⁻¹ resolution. The degree of photodegradation of LDPE films was evaluated by determining the presence of carbonyl (C \rightleftharpoons O) and vinyl (CH₂ \rightleftharpoons CH₂) groups at the wavenumbers of 1715 cm⁻¹ and 909 cm $^{-1}$, respectively. On the other hand, photodegradation of PET was determined from the comparative spectra and carboxyl index (CXI). The carbonyl index (CI), vinyl index (VI) and CXI were calculated as described in SI-3. The X-ray photoelectron spectroscopy (XPS) measurements of photodegraded LDPE and PET were performed using a Thermo Scientific Spectrometer XPS equipped with a monochromatic Al K α radiation (h ν = 1486.6 eV) with an X-ray source operating power of 75 W at 12 kV. More information is provided in SI-3. The surface wettability alterations of the MPs due to the photodegradation were characterized by the water contact angle measurements. The Biolin Scientific Attention Tetha attached with Vivitar lenses was used to measure the water contact angles. LDPE and PET MP samples were mounted on a glass slide with double-sided clear tape. The water was used as a sessile drop, and it was Millipore grade with pH 7.0. For all the measurements three replicates were used.

2.5. Surface morphology characterizations

The Field Emission Scanning Electron Microscopy (FE-SEM) imaging was employed to evaluate the surface morphology of MPs due to the photo and mechanical degradations. An FEI Nova NanoSEM 650 attached with Oxford X-Max $^{\rm N}$ Silicon Drift detector was used at 10 kV with uniform 2500 \times magnification. More information is provided in SI-4. The alterations of MPs' surface roughness due to the photodegradation were examined using an Atomic Force Microscopy (AFM Workshop, TT-AFM). The scanning rate was 0.5 Hz with tapping mode and a silicon probe was used with a constant force of 58 N/m on a scan area of 25 μm^2 for a sample at room temperature. The average roughness (nm), $R_{\rm av}$ was calculated using Equation (1) (Aghilinasrollahabadi et al., 2020) where N defines the number of observed heights (nm), Z_i is the corresponding height (nm), and \overline{Z} defines the average height (nm).

$$R_{av} = \sum_{i=1}^{N} \frac{|Z_i - \overline{Z}|}{N} \tag{1}$$

2.6. Lead exposure experiments and kinetics modeling

The new and 48 d photodegraded LDPE and PET MPs were exposed to Pb solution at pH = 7.0, using synthetic stormwater in the 50 mL polytetrafluoroethylene (PTFE) bottles. The chemical composition of the synthetic stormwater is listed in Table SI-1 (Aghilinasrollahabadi et al., 2020). Kinetic experiments were conducted exposing MPs to 300 $\mu g/L$ Pb solution for six (2, 6, 12, 24, 48, and 120 h) time intervals at 21.6 \pm

1 °C. Eight MPs were added to a 12 mL of Pb solution (surface/volume ratio of 1:3 cm²/mL) in a 50 mL PTFE bottle and three replicates were used for each sample (each time interval). The MPs were removed from the exposed solutions with tweezers at different time intervals and digested in 10 mL of 2% nitric acid for at least 24 h. Only for few of the bottles, the 48 d photodegraded LDPE MPs were broken into smaller pieces, in which they were separated using the 11 µm pore size filter paper. However, for reporting the metal accumulation data it was assumed that surface area was constant through the experiments. The kinetics of Pb adsorption onto the new and photodegraded LDPE and PET MPs were examined through pseudo 1st and 2nd order kinetics models. The pseudo 1st order kinetics model best describes the physical adsorption, however, the pseudo 2nd order kinetics model best describes the adsorption process where chemical association occurs between adsorbents and adsorbate species (Ahamed et al., 2020). Information regarding the Pb quantification and statistical analysis is provided in SI-6 and SI-7, respectively.

3. Results and discussions

3.1. Surface chemistry alterations of MPs due to the photodegradation

(A) ATR-FTIR spectroscopy: The ATR-FTIR spectra of new LDPE MPs demonstrated the asymmetric and symmetric bands of C-H stretching at 2915 and 2845 cm⁻¹, respectively. The asymmetric and symmetric bending vibrations of CH_2 appeared at 1467 and 1462 cm⁻¹. The peaks due to the bending vibrations of CH₃ and rocking vibrations of CH₂ appeared at 1377 cm⁻¹ and 730 cm⁻¹, respectively (Fig. 1) (Babaghayou et al., 2016). The new peaks appeared at 1715 cm⁻¹ and 909 cm⁻¹, representing the carbonyl (C=O) and vinyl (CH=CH) groups, for LDPE MPs after UVB irradiation for 21 d and 48 d (Martínez-Romo et al., 2015). The carbonyl and vinyl indices for new LDPE MPs were increased from 0.0 to 1.9 and from 0.1 to 1.1, respectively, after 21 d of UVB radiation. The 48 d of UVB exposure has increased the carbonyl index to 2.91 and vinyl index to 1.92. Our results were confirmed by prior studies that reported increased carbonyl and vinyl indices with exposure time for LDPE films exposed to sunlight up to 21 months (Babaghayou et al., 2016; Chabira et al., 2008).

The photodegradation of LDPE initiates by absorbing the UV radiation due to the chromophoric defects present in the polymer structure. The UVB radiation (wavelength 360-280 nm with a peak at 313 nm) has sufficient energy (90.86–102.11 kcal/mol) to break down the chemical bonds in LDPE (e.g., C–C \rightarrow 77–83 kcal/mol; C–H \rightarrow 94–99 kcal/mol)

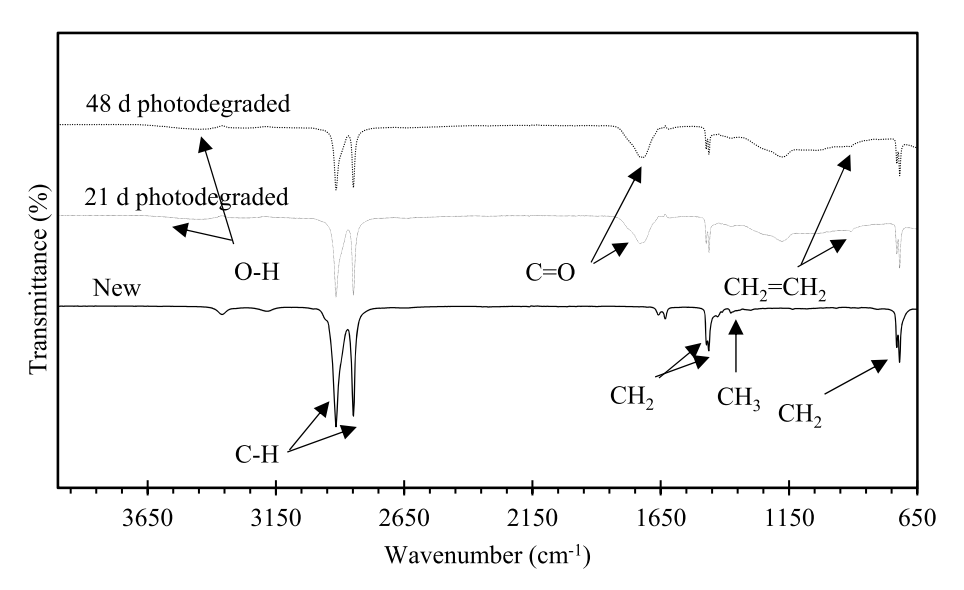


Fig. 1. ATR-FTIR spectra of new, 21 d, and 48 d UVB exposed LDPE MPs.

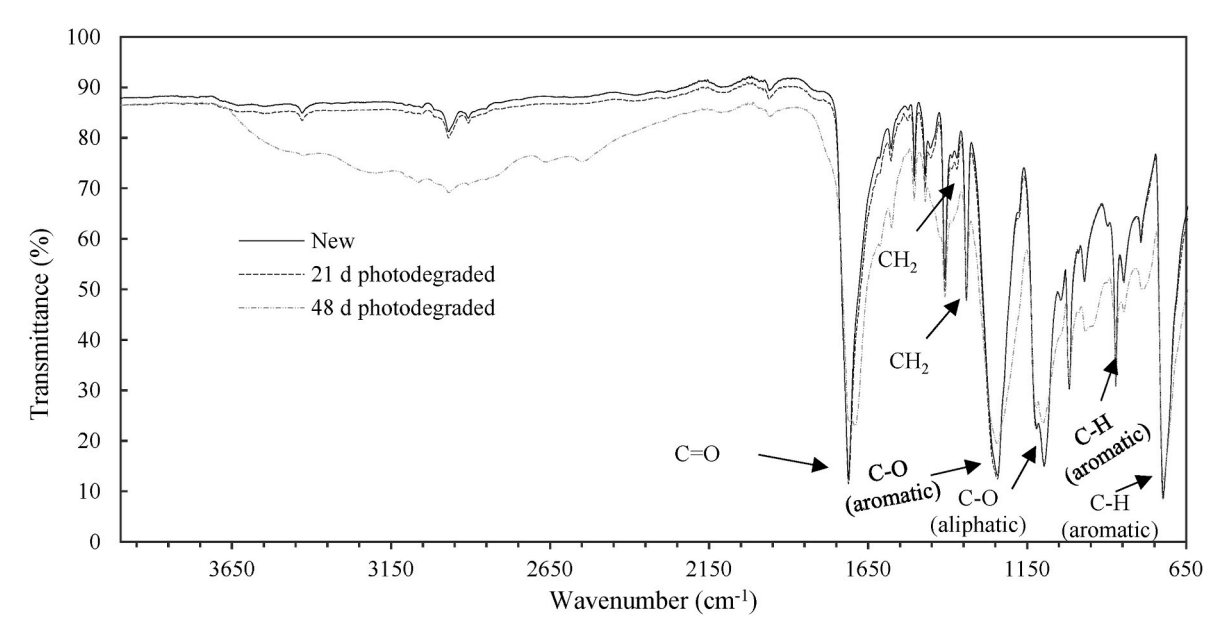


Fig. 2. ATR-FTIR spectra of new, 21 d, and 48 d photodegraded PET MPs.

(Rånby, 1989; Pickett et al., 2008). Thus, the hydrogen abstraction may occur following the UV absorbance, which leads to the formation of radicals, intermediate hydroperoxide products, and finally, the carbonyl groups (Krehula et al., 2014). Additional UV exposure causes the carbonyl functional groups to follow the Norrish type I and/or Norrish type II reactions which leads to the chain scission. In the Norrish type I reaction, the chain scission is caused by the cleavage of a C–C bond which results in the formation of two free radicals to be reacted and create the fragments of the polymer chain. The Norrish type II reaction also causes the chain scission by forming vinyl groups and diradical moiety within the chain (Singh and Sharma, 2008).

The ATR-FTIR spectra of new and photodegraded PET MPs are shown in Fig. 2. The main peaks of the new PET MPs appeared at 1713 cm⁻¹ and 1370 cm⁻¹, representing the carbonyl (C=O) and gauche wagging CH₂, respectively. The trans wagging CH₂ and aromatic ether (C-O) were found at 1340 cm⁻¹ and 1241 cm⁻¹. The bands that appeared at 1094 cm⁻¹, 870 cm⁻¹, and 720 cm⁻¹ demonstrated the aliphatic ether (C-O), aromatic out of plane wagging C-H, and aromatic in-phase wagging C-H, respectively (Joakeimidis et al., 2016). Decreasing the intensity of all characteristic peaks of PET MPs (except gauche wagging CH₂) due to the UVB radiation indicates the possible photodegradation of this polymer (Lee et al., 2012). This result is

confirmed by other studies which reported decreasing the peak intensity for carbonyl or ketone, aromatic ether, aliphatic ether, aromatic out of the plane, and in-phase wagging C-H, due to the photodegradation of PET bottles in the marine environment (Ioakeimidis et al., 2016). As reported in the literature, the carboxyl end groups are forming due to the photodegradation of PET (Blais et al., 1973), thus, further information regarding the extent of PET photodegradation can be inferred from the magnitude of the carboxyl index (CXI). The carboxyl end groups are expediting further degradation of PET (Fechine et al., 2002). The 21 d UVB radiation of PET MPs increased the carboxyl index for the new PET MPs from 0.67 to 0.71. Additional exposure to UVB radiation (up to 48 d) increased CXI to 0.78. The CXI value increased from 56.1% to 73.2% after 21 and 48 days, respectively, of UVB exposed compared to the new PET. The broad peak appeared approximately from 3650 to 2150 cm⁻¹ on ATR-FTIR spectra of 48 d UVB irradiated PET MPs can be assigned to the -OH vibration of the -COOH functions in carboxylic acid end groups that were generated by further degradation and chain scission of PET (Fechine et al., 2004; Rodriguez et al., 2020). The literature suggested the Norrish Type II pathway for photodegradation of PET in the air (Blais et al., 1973; Fechine et al., 2004). In this process, hydrogen abstraction occurs and results in the generation of initial radicals. Then hydroxyl and alkoxy radicals are being generated through photolysis of

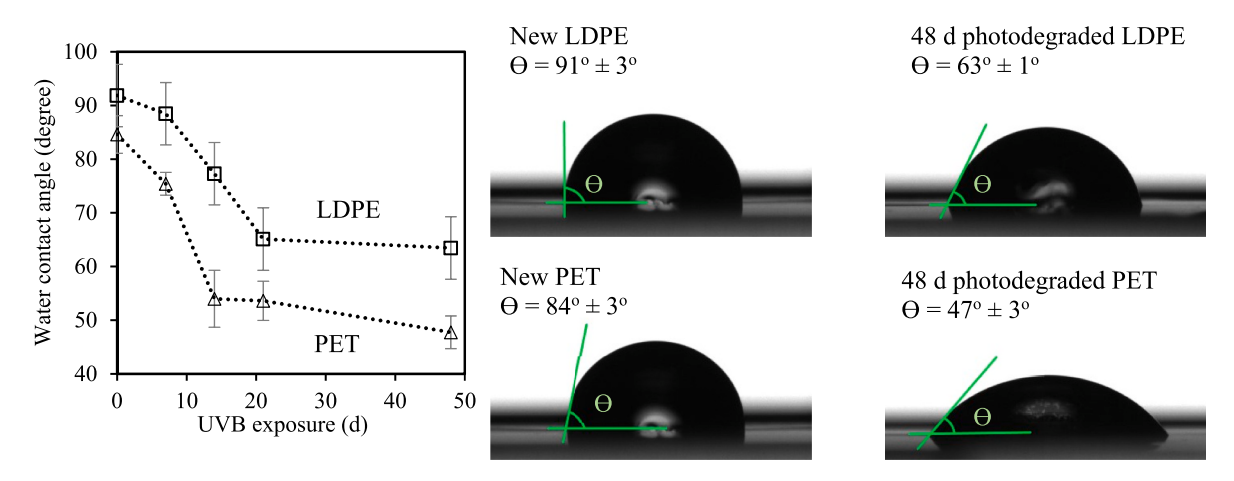


Fig. 3. Water contact angle analysis of new and UVB exposed LDPE and PET MPs.

hydroperoxides. These hydroxyl radicals substitute in the phenylene ring to generate the monohydroxy terephthalate groups in the polymeric chain (Day and Wiles, 1972). The schematics of photodegradation processes for LDPE and PET are shown in **Schematic SI-1** and **Schematic SI-2**.

(B) XPS analysis: The XPS survey spectra and high-resolution C 1s spectra for new and UVB exposed LDPE and PET MPs are shown in Figure SI-1 and Figure SI-2, respectively. For both polymers, the C1s peak at 284.6-284.7 eV was the dominant feature associated with the LDPE and PET chemical structures (Salehi et al., 2018). The O 1s peak for both new LDPE and PET samples was found at 532.1-534.1 eV binding energy (Herath et al., 2022). The O 1s peaks for the new LDPE and PET MPs could be due to their intrinsic surface oxidation (Salehi et al., 2018). As expected, the percentage of oxygen for photodegraded LDPE and PET samples was greater compared to the new samples, confirming their photooxidations due to the UVB exposure. The ratios of oxygen to carbon (O/C) and oxidized carbon to unoxidized carbon (Cox/Cunox) demonstrate an ascending trend of oxygen content with increasing the duration of UVB exposure for both LDPE and PET MPs (Table SI-2). Analyzing the C 1s spectra revealed four types of oxidation states for carbon including C-C, C-O, C=O, and O-C=O for both 21 d and 48 d UVB exposed LDPE MPs. On the other hand, for the new, 21 d and 48 d UVB exposed PET MPs, three types of oxidation states were found for carbon as C-C, C-O, and O-C=O (Nand et al., 2012). Carboxylic (O-C=O) end groups could be generated on the PET surface through the Norrish Type II reactions where an intramolecular γ-hydrogen abstraction occurred creating a cyclic intermediate resulting from the polymer chain scission (Hurley and Leggett, 2009). The oxygen content on the surface of the PET MPs has increased with the increased duration of UVB exposure as the generated radicals reacted further with the surrounding atmospheric oxygen (Hurley and Leggett, 2009).

(C) Water contact angle analysis: Significant reductions of water contact angles were found for both LDPE and PET MPs due to the photodegradation (Fig. 3). The water contact angle for new LDPE MPs was reduced by 31% (from 91° to 63°) due to 48 d of UVB exposure. The water contact angle for new PET MPs was reduced by 44% (from 84° to 47°) due to 48 d of UVB exposure. The reduction in the water contact angles for LDPE MPs, compared to their new MPs, after 7 d, 14 d, and 21 d of UVB exposure were 4%, 16%, and 29%, respectively. Similarly, the water contact angles were reduced by 11%, 36%, and 37% for the PET MPs, after the same UVB exposure durations. Thus, increased duration of photodegradation promoted hydrophilicity for the two studied MPs. Generally, the surface wettability increases with increasing the surface roughness and developing the polar surface functional groups. The AFM analysis conducted in this study revealed the greater surface roughness of MPs with an increased duration of UVB exposure. The increased polarity of LDPE and PET MPs could be due to the formation of oxidized carbon and hydroxyl surface functional groups due to the UVB exposure as confirmed by ATR-FTIR spectroscopy (Holmes-Farley et al., 1988).

3.2. Surface morphology alterations of MPs due to the degradation experiments

(A) **FE-SEM Imaging:** The visual observations revealed opaque appearance for LDPE MPs and discoloration of clear PET MPs to yellowish as early as seven days of the UVB exposure. The FE-SEM images demonstrated the alteration of the smooth, homogenous, and compact surfaces of new LDPE and PET MPs, to the nonhomogeneous and rough surfaces after 48 d of UVB exposure (Fig. 4). Wrinkles and flakes were identified on the surface of LDPE and PET MPs after the 48 d of UVB exposure. This result of LDPE MPs is confirmed by Ranjan and Goel (2019) they reported an increased surface roughness and flakes formation on the LDPE surface after 30 d of UVB exposure (Ranjan and Goel, 2019). Other studies showed that the photodegradation of PET occurs by developing hydroperoxides, which produce free radicals to initiate degradation and contributes to surface roughnes (Feller, 1994;

Ferreira et al., 2021). Subsequent exposure of our 48 d photodegraded LDPE and PET MPs to the mechanical forces applied for 28 d through abrasion with sand particles resulted in creating network of cracks and granular texture on the surface of both MPs, however, the cracks on LDPE surfaces were wider and deeper than those on the PET MPs. The granular texture was generated mainly through sand/silt accumulated onto the plastic surfaces after the subsequent mechanical abrasion. As discussed in our recent study, during the accelerated mechanical degradation experiments, the sharp edge of sand/silt particles could abrade the plastic surface and create the resting space for penetration and further accumulation of smaller silt particles onto the MPs surface (Aghilinasrollahabadi et al., 2020). However, the lower hardness and greater plasticity of LDPE MPs (41-46 D) compared to the PET MPs (84 D) promoted its deformation by the sand/silt particles and enhanced the silt accumulation onto its surface (Aghilinasrollahabadi et al., 2020). The study conducted by Gewert et al. (2015) confirmed similar surface morphology alterations for LDPE and PET plastics those were degraded in natural solar radiation and under natural mechanical forces, where the LDPE plastics were found more brittle, degraded, and fragmented than PET samples (Gewert et al., 2015). Therefore, though both the polymer MPs were exposed to the similar duration of UVB exposure before subsequent mechanical abrasion, the LDPE MPs became more brittle than PET MPs, as reported by the previous studies (Iñiguez et al., 2018; Miranda et al., 2021), thus, LDPE MPs showed greater morphological changes than PET MPs after similar duration of subsequent mechanical degradation.

(B) Atomic Force Microscopy (AFM) analysis: The AFM analysis also confirmed the increases in surface roughness of LDPE and PET MPs with an increased duration of UVB exposure. Figure SI-3 shows the slight increases in surface roughness of photodegraded LDPE and PET MPs compared to their new MPs. After 21 d of UVB exposure, the surface roughness of new LDPE and PET MPs was increased from 30.3 to 35.6 nm and from 1.9 to 2.1 nm, respectively. However, after 48 d of UVB exposure, the surface roughness of LDPE and PET MPs were increased to 52.20 nm and 7.00 nm, respectively (Figure SI-3). The FE-SEM images confirmed this finding by demonstrating the generation of nonhomogeneous and rough MPs surfaces after UVB exposure. This increased roughness could be due to photoinduced reactions that occurred during the UVB exposure (Ali et al., 2016). The FE-SEM images of UVB exposed and mechanically weathered MPs also clearly demonstrated significant changes of surface morphology, that could be mainly due to the silt/sand accumulation onto the MPs due to the mechanical weathering process. Our recent study also demonstrated an increased surface roughness for MPs that were mechanically weathered using a similar procedure (Aghilinasrollahabadi et al., 2020).

3.3. MPs fragmentation due to the combined photo and mechanical degradations

The mechanical disintegration of plastics into smaller segments is defined as fragmentation. In this study, the degree of fragmentation of new and 48 d photodegraded LDPE and PET MPs were examined by applying the abrasive wear forces as they were shaken with the sand particles to simulate their abrasion with the sediments present in the road deposits. Surface abrasion is reported by literature as one of the primary mechanisms contributing to the generation of many daughter fragments following the plastic weathering (Song et al., 2017; Sun et al., 2020). As we described in our recent study, the abrasion of plastics with the sharp edge of sand particles could generate grooves, scratches, and the network of microcracks onto the surface of the plastic (Aghilinasrollahabadi et al., 2020). The repetitive process of plastics abrasion with sand particles resulted in penetration of these microcracks into the plastic structure and $% \left(1\right) =\left(1\right) \left(1\right$ subsequently chipping of the small plastic fragments, as shown in Fig. 5. The results demonstrated that after 28 d of mechanical degradation experiments, a greater number of fragments were generated from a single 21 d UVB exposed LDPE MPs (3986 \pm 706) and PET (3179 \pm 751) MPs

compared to a single new LDPE MPs (2250 \pm 233) and PET MPs (1549 \pm 171) (p-value < 0.05) (Fig. 6). Despite the significant increase in the number of fragments generated by 48 d UVB exposed LDPE MPs (8397 \pm 2259) compared to the 21 d UVB exposed MPs (p-value < 0.05), the number of fragments released from 48 d UVB exposed PET MPs (4238 \pm 1002) was not significantly increased compared to the 21 d UVB exposed PET MPs (p-value > 0.05) (Fig. 6). The order of LDPE_{uv48d} > PET_{uv48d} > $LDPE_{uv21d} > PET_{uv21d} > LDPE_{new} > PET_{new}$ in terms of fragments generated after 28 d of mechanical degradation was found. Loss of plastics' mechanical properties due to the photodegradation in combination with applied shear forces and tensile stresses have been suggested in the literature to result in plastic fragmentation (Ter Halle et al., 2016). The weakening, breakage, and shortening of the polymeric chain backbone and leaching of plasticizers due to the UVB irradiation make the plastics more brittle, and subsequent exposure to mechanical forces accelerate the formation of cracks and surface defects to the plastics (Chubarenko et al., 2020; Song et al., 2017). Formation of a greater degree of surface cracks stimulates the generation of plastic fragments as these cracks connect and chip off the debris (Gerritse et al., 2020). Our visual observations showed that the erosion of MPs mainly occurred around their edges. The greater number of fragments generated by LDPE MPs compared to PET MPs can be explained by the physical and mechanical properties of these polymers. The LDPE film (0.913 g/cm³) was less dense than the PET film (1.384 g/cm³). Therefore, LDPE was more susceptible to being torn apart when exposed to mechanical force as loosely packed material is more likely to fragmentation compared to the densely packed material (Song et al., 2017). In addition, LDPE's lower hardness and tensile strength (41-46 D and 9.65-21.99 MPa) compared to the PET (84 D and 193.05 MPa) could be responsible for its more significant fragmentation. Despite the similar duration of UVB exposure, the LDPE MPs became more brittle than PET, as reported by the previous studies (Iñiguez et al., 2018; Miranda et al., 2021). Therefore, LDPE MPs generated a greater number of fragments due to the combined photo and mechanical degradations than PET MPs.

The diameter of 84.8% of the fragments generated by mechanical degradation of new LDPE MPs varied between 10 μ m and 30 μ m (Fig. 7a). However, the diameter of 15.2% of these generated fragments was between 30 μ m and 120 μ m. This size distribution was slightly changed for the fragments generated from 21 d to 48 d UVB exposed LDPE MPs. The diameter of 79.6% and 75.8% of generated LDPE fragments was between 10 μ m and 30 μ m, respectively, for 21 d and 48

d UVB exposed LDPE MPs (Fig. 7a). On the other hand, the diameter of 80.5% of the fragments generated from new PET MPs varied from $10~\mu m$ to 30 μ m, and only the diameter of 19.5% of the generated fragments varied from 30 μm to 120 μm (Fig. 7b). This size distribution was slightly changed for the fragments generated from 21 d to 48 d UVB exposed PET MPs. The diameter of 90.0% and 85.7% of generated PET fragments were between 10 µm and 30 µm, respectively, 21 d and 48 d UVB exposed PET MPs (Fig. 7b). As reported by the literature, the photodegradation made the LDPE MPs more brittle than PET MPs (Iñiguez et al., 2018; Miranda et al., 2021); therefore, the implemented accelerated mechanical degradation resulted in the generation of the greater number of larger diameter fragmented particles from LDPE MPs than PET MPs. Future quantification of polymeric chain scissions, plasticizers leaching, and tensile strength variations due to the UVB radiation could promote understanding of photodegraded LDPE and PET MPs fragmentation behavior. The size of generated MPs is very critical as it determines their transport mechanism within the environment, potential ecological hazards, and contaminant transport behavior. The larger surface of smaller MPs provides a greater number of adsorption sites for the contaminant accumulation. Furthermore, the greater degree of LDPE MPs fragmentation could be due to their lower density, hardness, and tensile strength compared to the PET MPs (Song et al., 2017).

3.4. The kinetics of lead (Pb) uptake by new and photodegraded MPs

In this study, the kinetics of Pb adsorption onto the new and 48 d UVB exposed LDPE and PET MPs were investigated through the fiveday metal exposure experiments. The results revealed a significantly greater (p-value < 0.05) level of Pb surface accumulation onto the photodegraded LDPE MPs compared to the new samples (Fig. 8a). During the first 2 h of Pb exposure, the photodegraded LDPE MPs accumulated 47.3% of their equilibrium Pb surface loadings, while the new LDPE MPs obtained 53.6%. However, the equilibrium Pb surface loading on photodegraded LDPE MPs (2264 µg/m²) was almost five folds greater than the new samples (464 μ g/m²). The Pb accumulation onto the new LDPE MPs followed the pseudo 1st order kinetic model (r² = 0.98) as the adsorption of Pb occurred mostly through the mass transfer process with presumably no chemical association occurring (Salehi et al., 2018). However, the oxidized carbon functional groups (C-O, C=O, O-C=O) present on the 48 d photodegraded LDPE surface promoted the accumulation of the positively charged Pb species present

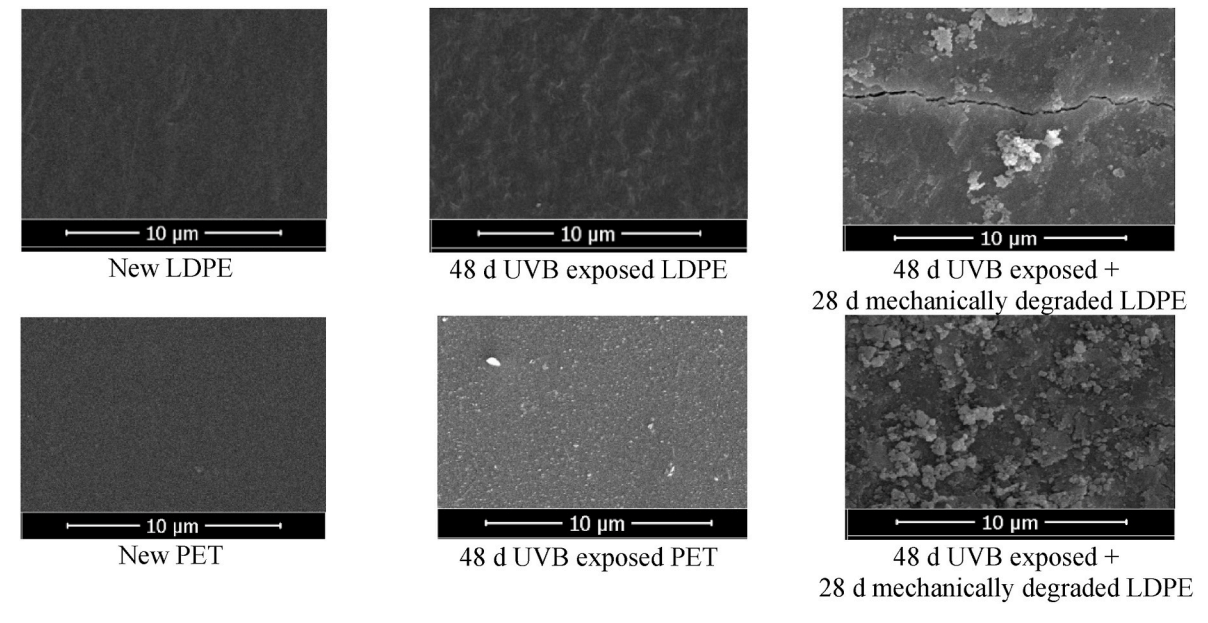


Fig. 4. FE-SEM images of new, 48 d UVB exposed, and 48 d UVB exposed +28 d mechanically degraded MPs.

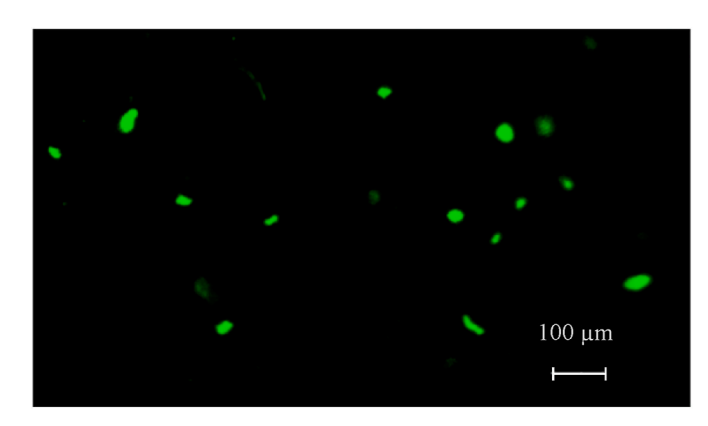


Fig. 5. The fluorescence microscopy image of the fragments generated by 28 d of mechanical degradation of 48 d photodegraded LDPE.

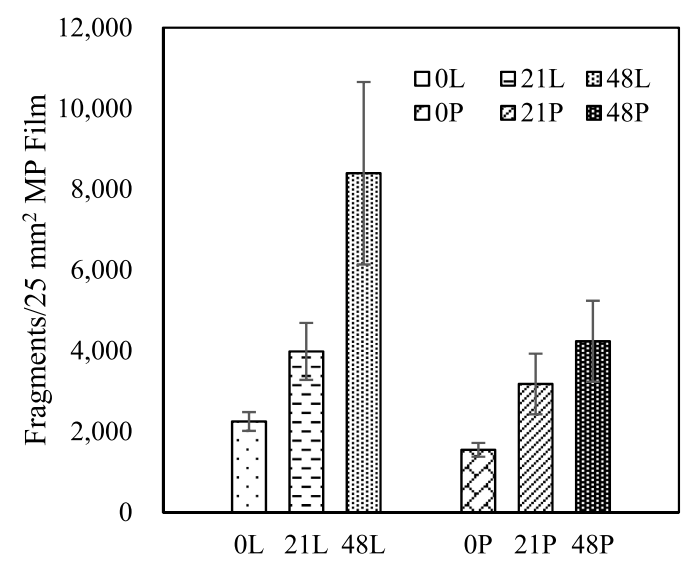
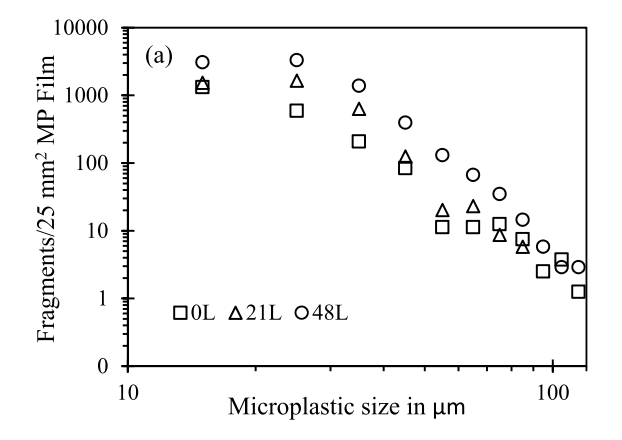


Fig. 6. The number of fragments generated by 28 d of mechanical degradation of new (0 L), 21 d (21 L) and 48 d (48 L) photodegraded LDPE, and new (0 P), 21 d (21 P), and 48 d (48 P) photodegraded PET MPs.

in the synthetic stormwater through surface complexation (Ou et al., 2019), and/or electrostatic attractions (Gao et al., 2021). Therefore, the pseudo 2nd order kinetic model ($r^2 = 0.92$) best described the Pb uptake by the photodegraded LDPE MPs. Increased accumulation of Pb species onto degraded polymeric surfaces has been reported previously, attributing to the increased specific surface area (Gallowaya and Lewisa, 2016), presence of polar functional groups, and increased hydrophilicity (Fotopoulou and Karapanagioti, 2012). The half-life $(t_{1/2})$, from the pseudo 1st order kinetic model, for Pb species was longer for the photodegraded LDPE MPs (8.9 h) than the new LDPE MPs (7.1 h) (Table SI-3). The maximum Pb accumulation onto the photodegraded LDPE MPs was found as 25.5% and for new LDPE MPs was found as 5.2% of the total Pb present in the synthetic stormwater. The Pb surface loading onto the new PET MPs after 2 h of metal exposure was found as $136 \text{ ug/m}^2 (1.51\% \text{ of Pb}_t)$ and increased to the maximum of 265 ug/m^2 (2.94% of Pb_t) after 6 h of the exposure. This Pb surface loading was gradually decreased to $21 \,\mu\text{g/m}^2$ after five-day of exposure (Fig. 8b). The maximum Pb adsorption onto the photodegraded PET MPs was found as 1314 µg/m² (14.60% of Pb_t) after 24 h exposure. This Pb surface loading gradually decreased to 725 µg/m² (8.05% of Pb_t) after five-day exposure period (Fig. 8b). The greater level of Pb accumulation onto the photodegraded PET MPs, compared to the new PET MPs, could be due to the presence of carboxyl (O-C=O) group on their surface, which promoted electrostatic interaction, surface complexation and/or surface coordination with the Pb species present in the aqueous solution (Gallowaya and Lewisa, 2016). However, we were not able to fit neither the pseudo 1st order nor the pseudo 2nd order kinetic model to the Pb adsorption data for both new and photodegraded PET MPs, similar to the study conducted by Coskun and Soykan (2006). Godov et al. (2019) also showed a lower adsorption capacity of heavy metals onto PET compared to polyethylene (Godoy et al., 2019). Our further investigation demonstrated a significantly greater Pb surface loadings (p-value < 0.05) onto the 48 d UVB exposed LDPE (2237 \pm 225 $\mu g/m^2)$ and PET MPs (1084 \pm 108 $\mu g/m^2$) compared to the 21 d UVB exposed LDPE (783 \pm 140 $\mu g/m^2$) and PET MPs (834 \pm 88 $\mu g/m^2$), respectively (Figure SI-4). These greater Pb surface loadings could be explained by the presence of greater percentages of oxidized carbon functional groups onto the 48 d UVB exposed LDPE MPs (14.3%) compared to the 21 d UVB exposed LDPE MPs (19.2%) as discussed in XPS analysis. Furthermore, the greater carboxyl index of 48 d UVB exposed PET (0.78) compared to the 21 d UVB exposed PET MPs (0.71), also indicates the greater polarity of the plastic surface due to the longer UVB exposure, which promoted the electrostatic interaction and coordination with the Pb species.



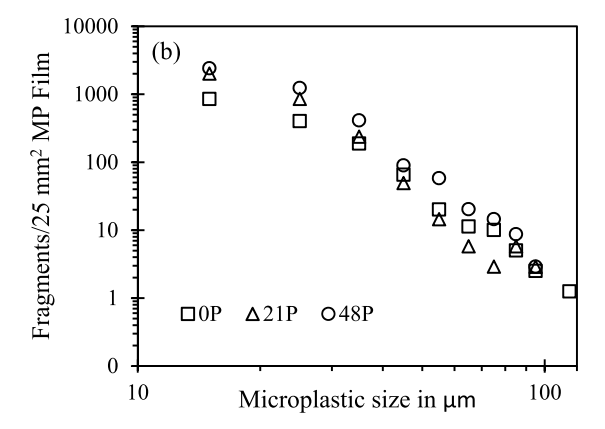
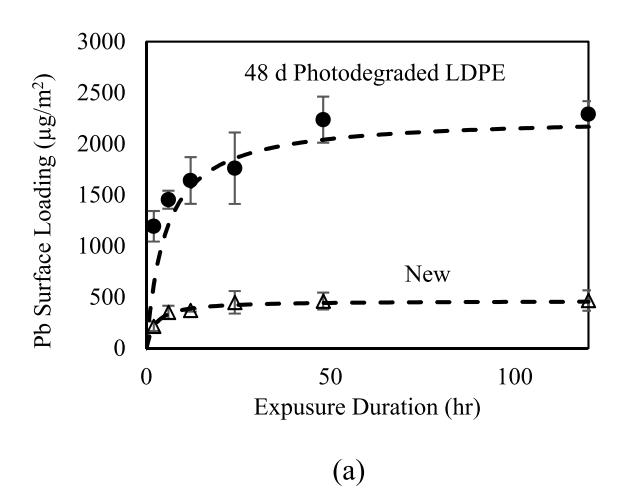


Fig. 7. The size distribution of plastic fragments generated by 28 d of mechanical degradation for (a) new (0 L), 21 d (21 L), and 48 d (48 L) photodegraded LDPE and (b) new (0 P), 21 d (21 P), and 48 d (48 P) photodegraded PET MPs.



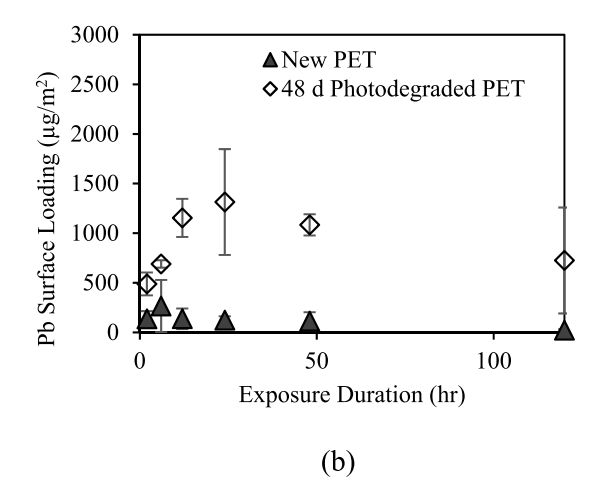


Fig. 8. (a) The pseudo 2nd order kinetics model and experimental Pb surface loadings for new and photodegraded LDPE MPs, and (b) Pb surface loading on New and photodegraded PET MPs.

4. Conclusion

In this study, the fate and contaminant transport behavior of LDPE and PET MPs as the model urban litter were investigated. Calculation of carbonyl and carboxyl indices for the UVB exposed LDPE and PET MPs demonstrated an increased degree of photodegradation over longer UVB exposure periods. The photodegradation of both LDPE and PET MPs increased the degree of their fragmentation by making them more brittle. A greater number of fragments were released from the new and photodegraded LDPE MPs compared to new and photodegraded PET MPs. The kinetics study demonstrated a greater level of Pb accumulation onto the photodegraded LDPE and PET MPs compared to the new MPs. With the rapidly growing consumption of plastic products and an increasing number of intensive storm events, it is critical to develop effective municipal policies and initiatives to limit and control the extent of this plastic pollutant released to the urban environment, particularly in areas of low socioeconomic status and urban communities where there is little awareness of environmental pollution. This study will inform necessary changes in regulatory systems to address MPs release to storm runoff. Implementing plastic pollution control policies could be promoted through effective social engagements and motivations.

Declaration of competing interest

The authors declare that they have no known competing financial interests or personal relationships that could have appeared to influence the work reported in this paper.

Acknowledgment

The authors would like to thank Dr. Felio Perez, Dr. Omar Skalli, Tanvir Ahmed, and Khashayar Aghilinasrollahabadi for their assistance during experiments or sample analysis. Funding for this work was provided by the National Science Foundation grant CBET-2044836 and the United States Department of Agriculture, National Institute of Food and Agriculture, USDA/NIFA) Award number 2020-67019-31166.

Appendix A. Supplementary data

Supplementary data to this article can be found online at https://doi. org/10.1016/j.envres.2022.113183.

References

- Abdolazimi, O., Salehi Esfandarani, M., Salehi, M., Shishebori, D., Shakhsi-Niaei, M., 2021. Development of sustainable and resilient healthcare and non-cold pharmaceutical distribution supply chain for COVID-19 pandemic: a case study. Int. J. Logist. Manag. https://doi.org/10.1108/IJLM-04-2021-0232.
- Aghilinasrollahabadi, K., Salehi, M., Fujiwara, T., 2020. Investigate the influence of microplastics weathering on their heavy metals uptake in stormwater. J. Hazard Mater. 408, 124439. https://doi.org/10.1016/j.jhazmat.2020.124439.
- Ahamed, T., Brown, S.P., Salehi, M., 2020. Investigate the role of biofilm and water chemistry on lead deposition onto and release from polyethylene: an implication for potable water pipes. J. Hazard Mater. 400, 123253. https://doi.org/10.1016/j. ibazmat.2020.123253.
- Ali, S.S., Qazi, I.A., Arshad, M., Khan, Z., Voice, T.C., Mehmood, C.T., 2016. Photocatalytic degradation of low density polyethylene (LDPE) films using titania nanotubes. Environ. Nanotechnol. Monit. Manag. 5, 44–53. https://doi.org/ 10.1016/j.enmm.2016.01.001.
- Babaghayou, M.I., Mourad, A.H.I., Lorenzo, V., et al., 2016. Photodegradation characterization and heterogeneity evaluation of the exposed and unexposed faces of stabilized and unstabilized LDPE films. Mater. Des. 111, 279–290. https://doi.org/ 10.1016/j.matdes.2016.08.065.
- Ballent, A., Corcoran, P.L., Madden, O., Helm, P.A., Longstaffe, F.J., 2016. Sources and sinks of microplastics in Canadian Lake Ontario nearshore, tributary and beach sediments. Mar. Pollut. Bull. 110 (1), 383–395. https://doi.org/10.1016/j. marpolbul.2016.06.037.
- Blais, P., Day, M., Wiles, D.M., 1973. Photochemical degradation of poly(ethylene terephthalate). IV. Surface changes. J. Appl. Polym. Sci. 17, 1895–1907. https://doi.org/10.1002/app.1973.070170622.
- Chabira, S.F., Sebaa, M., G'sell, C., 2008. Influence of climatic ageing on the mechanical properties and the microstructure of low-density polyethylene films. J. Appl. Polym. Sci. 110 (4), 2516–2524. https://doi.org/10.1002/app.28823.
- Chubarenko, I., Efimova, I., Bagaeva, M., Bagaev, A., Isachenko, I., 2020. On mechanical fragmentation of single-use plastics in the sea swash zone with different types of bottom sediments: insights from laboratory experiments. Mar. Pollut. Bull. 150, 110726. https://doi.org/10.1016/J.MARPOLBUI.2019.110726.
- Coskun, R., Soykan, C., 2006. Lead(II) adsorption from aqueous solution by poly (ethylene terephthalate)-g-acrylamide fibers. J. Polym. Res. 13 (1), 1–8. https://doi. org/10.1007/s10965-005-9000-3.
- Day, M., Wiles, D.M., 1972. Photochemical degradation of poly(ethylene terephthalate).
 III. Determination of decomposition products and reaction mechanism. J. Appl.
 Polym. Sci. 16 (1), 203–215. https://doi.org/10.1002/app.1972.070160118.
- Dehghani, S., Moore, F., Akhbarizadeh, R., 2017. Microplastic pollution in deposited urban dust, Tehran metropolis, Iran. Environ. Sci. Pollut. Res. 24 (25), 20360–20371. https://doi.org/10.1007/s11356-017-9674-1.
- DeSimone, D., Sharafoddinzadeh, D., Salehi, M., 2020. Prediction of children's blood lead levels from exposure to lead in schools' drinking water—a case study in Tennessee, USA. Water 12 (6), 1826. https://doi.org/10.3390/w12061826.
- Devriese, L.I., Witte, B De, Vethaak, A.D., Hostens, K., Leslie, H.A., 2017. Chemosphere Bioaccumulation of PCBs from microplastics in Norway lobster (Nephrops norvegicus): an experimental study. Chemosphere 186, 10–16. https://doi.org/10.1016/j.chemosphere.2017.07.121.
- Enfrin, M., Lee, J., Gibert, Y., Basheer, F., Kong, L., Dumée, L.F., 2020. Release of hazardous nanoplastic contaminants due to microplastics fragmentation under shear

- stress forces. J. Hazard Mater. 384 (September 2019), 121393. https://doi.org/ 10.1016/j.jhazmat.2019.121393.
- Fechine, G.J.M., Rabello, M.S., Souto-Maior, R.M., 2002. The effect of ultraviolet stabilizers on the photodegradation of poly(ethylene terephthalate). Polym. Degrad. Stabil. 75 (1), 153–159. https://doi.org/10.1016/S0141-3910(01)00214-2.
- Fechine, G.J.M., Rabello, M.S., Souto Maior, R.M., Catalani, L.H., 2004. Surface characterization of photodegraded poly(ethylene terephthalate). The effect of ultraviolet absorbers. Polymer 45 (7), 2303–2308. https://doi.org/10.1016/j. polymer.2004.02.003.
- Feller, R.E., 1994. The Getty Conservation Institute Accelerated Aging. Photochemical and Thermal Aspects.
- Ferreira, M.M., da Silva, E.A., Cotting, F., Lins, V. de FC., 2021. UV weathering and performance of a novel corrosion protective coating on steel made from recycled polyethylene terephthalate (PET). Corrosion Eng. Sci. Technol. 56 (3), 199–209. https://doi.org/10.1080/1478422X.2020.1836880.
- Fotopoulou, K.N., Karapanagioti, H.K., 2012. Surface properties of beached plastic pellets. Mar. Environ. Res. 81, 70–77. https://doi.org/10.1016/j. marenyres.2012.08.010.
- Gallowaya, T.S., Lewisa, C.N., 2016. Marine microplastics spell big problems for future generations. Proc. Natl. Acad. Sci. Unit. States Am. 113 (9), 2331–2333. https://doi. org/10.1073/PNAS.1600715113.
- Gao, X., Hassan, I., Peng, Y., Huo, S., Ling, L., 2021. Behaviors and influencing factors of the heavy metals adsorption onto microplastics: a review. J. Clean. Prod. 319, 128777. https://doi.org/10.1016/J.JCLEPRO.2021.128777.
- Geronimo, F.K.F., Maniquiz-Redillas, M.C., Tobio, J.A.S., Kim, L.H., 2014. Treatment of suspended solids and heavy metals from urban stormwater runoff by a tree box filter. Water Sci. Technol. 69 (12), 2460–2467. https://doi.org/10.2166/WST.2014.150.
- Gerritse, J., Leslie, H.A., de Tender, C.A., Devriese, L.I., Vethaak, A.D., 2020. Fragmentation of plastic objects in a laboratory seawater microcosm. Sci. Rep. 10 (1), 1–16. https://doi.org/10.1038/s41598-020-67927-1.
- Gewert, B., Plassmann, M.M., Macleod, M., 2015. Pathways for degradation of plastic polymers floating in the marine environment. Environ Sci Process Impacts 17 (9), 1513–1521. https://doi.org/10.1039/C5EM00207A.
- Godoy, V., Blázquez, G., Calero, M., Quesada, L., Martín-Lara, M.A., 2019. The potential of microplastics as carriers of metals. Environ. Pollut. 255 (Pt 3), 113363. https://doi.org/10.1016/J.ENVPOL.2019.113363.
- Herath, A., Salehi, M., Jansone-Popova, S., 2022. Production of polyacrylonitrile/ionic covalent organic framework hybrid nanofibers for effective removal of chromium (VI) from water. J. Hazard Mater. 427 (October 2021), 128167. https://doi.org/ 10.1016/j.jhazmat.2021.128167.
- Holmes, L.A., Turner, A., Thompson, R.C., 2012. Adsorption of trace metals to plastic resin pellets in the marine environment. Environ. Pollut. 160 (1), 42–48. https://doi. org/10.1016/J.ENVPOL.2011.08.052.
- Holmes-Farley, S.R., Bain, C.D., Whitesides, G.M., 1988. Wetting of functionalized polyethylene film having ionizable organic acids and bases at the polymer-water fnterface: relations between functional group polarity, extent of lonization, and contact angle with waterl. ACS Publ 4 (4), 921–937. https://doi.org/10.1021/ la00082a025
- Huang, X., Zemlyanov, D.Y., Diaz-Amaya, S., Salehi, M., Stanciu, L., Whelton, A.J., 2020. Competitive heavy metal adsorption onto new and aged polyethylene under various drinking water conditions. J. Hazard Mater. 385, 121585. https://doi.org/10.1016/ j.jhazmat.2019.121585.
- Hurley, C.R., Leggett, G.J., 2009. Quantitative investigation of the photodegradation of polyethylene terephthalate film by friction force microscopy, contact-angle goniometry, and X-ray photoelectron spectroscopy. ACS Appl. Mater. Interfaces 1 (8), 1688–1697. https://doi.org/10.1021/AM900250Q.
- Imhof, H.K., Schmid, J., Niessner, R., Ivleva, N.P., Laforsch, C., 2012. A novel, highly efficient method for the separation and quantification of plastic particles in sediments of aquatic environments. Limnol Oceanogr. Methods 10 (7), 524–537. https://doi.org/10.4319/lom.2012.10.524.
- Iñiguez, M.E., Conesa, J.A., Fullana, A., 2018. Recyclability of four types of plastics exposed to UV irradiation in a marine environment. Waste Manag. 79, 339–345. https://doi.org/10.1016/j.wasman.2018.08.006.
- Ioakeimidis, C., Fotopoulou, K.N., Karapanagioti, H.K., et al., 2016. The degradation potential of PET bottles in the marine environment: an ATR-FTIR based approach. Sci. Rep. 6 (March), 1–8. https://doi.org/10.1038/srep23501.
- Julienne, F., Delorme, N., Lagarde, F., 2019. From macroplastics to microplastics: role of water in the fragmentation of polyethylene. Chemosphere 236, 124409. https://doi. org/10.1016/J.CHEMOSPHERE.2019.124409.
- Kowalski, N., Reichardt, A.M., Waniek, J.J., 2016. Sinking rates of microplastics and potential implications of their alteration by physical, biological, and chemical factors. Mar. Pollut. Bull. 109 (1), 310–319. https://doi.org/10.1016/j. marpolbul.2016.05.064.
- Krehula, L.K., Katancić, Z., Siročić, A.P., Hrnjak-Murgić, Z., 2014. Weathering of high-density polyethylene-wood plastic composites. J. Wood Chem. Technol. 34 (1), 39–54. https://doi.org/10.1080/02773813.2013.827209.
- Lambert, S., Wagner, M., 2016. Formation of microscopic particles during the degradation of different polymers. Chemosphere 161, 510–517. https://doi.org/ 10.1016/j.chemosphere.2016.07.042.
- Lee, C.O., Chae, B., Kim, S Bin, Jung, Y.M., Lee, S.W., 2012. Two-dimensional correlation analysis study of the photo-degradation of poly(ethylene terephthalate) film. Vib. Spectrosc. 60, 142–145. https://doi.org/10.1016/j.vibspec.2011.10.013.
- Liu, F., Olesen, K.B., Borregaard, A.R., Vollertsen, J., 2019. Microplastics in urban and highway stormwater retention ponds. Sci. Total Environ. 671, 992–1000. https:// doi.org/10.1016/j.scitotenv.2019.03.416.

- Lundquist, L., Leterrier, Y., Sunderland, P., Manson, J.-A.E., 2000. Life Cycle Engineering of Plastics, first ed. Elsevier. https://doi.org/10.1016/B978-0-08-043886-3.X5000-6
- Martín, D.M., Ahmed, M.M., Rodríguez, M., García, M.A., Faccini, M., 2017. Aminated polyethylene terephthalate (PET) nanofibers for the selective removal of Pb(II) from polluted water. Mater 10, 1352. https://doi.org/10.3390/MA10121352, 2017;10 (12):1352
- Martínez-Romo, A., González-Mota, R., Soto-Bernal, J.J., Rosales-Candelas, I., 2015. Investigating the degradability of HDPE, LDPE, PE-BIO, and PE-OXO films under UV-B radiation. J Spectrosc 2015, 1–6. https://doi.org/10.1155/2015/586514.
- Miranda, M.N., Sampaio, M.J., Tavares, P.B., Silva, A.M.T., Pereira, M.F.R., 2021. Aging assessment of microplastics (LDPE, PET and uPVC) under urban environment stressors. Sci. Total Environ. 796, 148914. https://doi.org/10.1016/J. SCITOTENV.2021.148914.
- Nand, A.V., Ray, S., Travas-Sejdic, J., Kilmartin, P.A., 2012. Characterization of polyethylene terephthalate/polyaniline blends as potential antioxidant materials. Mater. Chem. Phys. 134 (1), 443–450. https://doi.org/10.1016/j. matchemphys.2012.03.015.
- Patrício Silva, A.L., Prata, J.C., Walker, T.R., et al., 2021. Increased plastic pollution due to COVID-19 pandemic: challenges and recommendations. Chem. Eng. J. 405, 126683. https://doi.org/10.1016/J.CEJ.2020.126683.
- Pickett, J.E., Gibson, D.A., Gardner, M.M., 2008. Effects of irradiation conditions on the weathering of engineering thermoplastics. Polym. Degrad. Stabil. 93 (8), 1597–1606. https://doi.org/10.1016/J.POLYMDEGRADSTAB.2008.02.009.
- Piñon-Colin, T. de J., Rodriguez-Jimenez, R., Rogel-Hernandez, E., Alvarez-Andrade, A., Wakida, F.T., 2020. Microplastics in stormwater runoff in a semiarid region, Tijuana, Mexico. Sci. Total Environ. 704, 135411. https://doi.org/10.1016/j. scitotenv. 2019.135411.
- Qu, C., Chen, W., Hu, X., et al., 2019. Heavy metal behaviour at mineral-organo interfaces: mechanisms, modelling and influence factors. Environ. Int. 131 (1), 104995. https://doi.org/10.1016/j.envint.2019.104995.
- Rånby, B., 1989. Photodegradation and photo-oxidation of synthetic polymers. J. Anal. Appl. Pyrolysis 15, 237–247. https://doi.org/10.1016/0165-2370(89)85037-5.
- Ranjan, V.P., Goel, S., 2019. Degradation of low-density polyethylene film exposed to UV radiation in four environments. J Hazardous, Toxic, Radioact Waste. 23 (4), 1–11. https://doi.org/10.1061/(asce)hz.2153-5515.0000453.
- Rodriguez, A.K., Mansoor, B., Ayoub, G., Colin, X., Benzerga, A.A., 2020. Effect of UV-aging on the mechanical and fracture behavior of low density polyethylene. Polym. Degrad. Stabil. 180, 109185. https://doi.org/10.1016/J. POLYMDEGRADSTAB.2020.109185.
- Salehi, M., 2022. Global water shortage and potable water safety; Today's concern and tomorrow's crisis. Environ. Int. 158 https://doi.org/10.1016/j.envint.2021.106936.
- Salehi, M., Jafvert, C.T., Howarter, J.A., Whelton, A.J., 2018. Investigation of the factors that influence lead accumulation onto polyethylene: implication for potable water plumbing pipes. J. Hazard Mater. 347, 242–251. https://doi.org/10.1016/j. ihazmat.2017.12.066.
- Salehi, M., Aghilinasrollahabadi, K., Esfandarani, M.S., 2020. An investigation of stormwater quality variation within an industry sector using the self-reported data collected under the stormwater monitoring program. Water (Switzerland) 12 (11), 1–16. https://doi.org/10.3390/w12113185.
- Schultz, P.W., Bator, R.J., Large, L.B., Bruni, C.M., Tabanico, J.J., 2013. Littering in context: personal and environmental predictors of littering behavior. Environ. Behav. 45 (1), 35–59. https://doi.org/10.1177/0013916511412179.
- Scott, D., Roof, V., Elder, B., 2020. Keep America Beautiful. National Litter Study.
 Shams, M., Alam, I., Mahbub, M.S., 2021. Plastic pollution during COVID-19: plastic waste directives and its long-term impact on the environment. Environ Adv 5, 105613. https://doi.org/10.1016/J.ENVADV.2021.100119.
- Singh, B., Sharma, N., 2008. Mechanistic implications of plastic degradation. Polym. Degrad. Stabil. 93, 561–584. https://doi.org/10.1016/j. polymdegradstab.2007.11.008.
- Song, Y.K., Hong, S.H., Jang, M., Han, G.M., Jung, S.W., Shim, W.J., 2017. Combined effects of UV exposure duration and mechanical abrasion on microplastic fragmentation by polymer type. Environ. Sci. Technol. 51 (8), 4368–4376. https:// doi.org/10.1021/acs.est.6b06155.
- Su, L., Nan, B., Craig, N.J., Pettigrove, V., 2020. Temporal and spatial variations of microplastics in roadside dust from rural and urban Victoria, Australia: implications for diffuse pollution. Chemosphere 252, 126567. https://doi.org/10.1016/j. chemosphere.2020.126567.
- Sun, Y., Yuan, J., Zhou, T., Zhao, Y., Yu, F., Ma, J., 2020. Laboratory simulation of microplastics weathering and its adsorption behaviors in an aqueous environment: a systematic review. Environ. Pollut. 265, 114864. https://doi.org/10.1016/j. envpol.2020.114864.
- Ter Halle, A., Ladirat, L., Gendre, X., et al., 2016. Understanding the fragmentation pattern of marine plastic debris. Environ. Sci. Technol. 50 (11), 5668–5675. https://doi.org/10.1021/acs.est.6b00594.
- Tesfaldet, Y.T., Ndeh, N.T., Budnard, J., Treeson, P., 2022. Assessing face mask littering in urban environments and policy implications: the case of Bangkok. Sci. Total Environ. 806, 150952. https://doi.org/10.1016/j.scitotenv.2021.150952.
- Vogelsang, C., Lusher, A., Dadkhan, M., et al., 2018. Microplastics in Road Dust Characteristics, Pathways and Measures, vol. 17.
- Wright, S.L., Kelly, F.J., 2017. Plastic and human health: a micro issue? Environ. Sci. Technol. https://doi.org/10.1021/acs.est.7b00423.